GRAVITATING MASSES OF POOR CLUSTERS OF GALAXIES

The paper appended here summarizes the work completed on this project during the referenced period.

NASA GRANT NAG5-2155

Semiannual and Final Reports
For the Period 15 December 1992 through 14 December 1995

Principal Investigator
Dr. Laurence P. David

September 1996

Prepared for:

National Aeronautics and Space Administration
Goddard Space Flight Center
Greenbelt, Maryland 20771

Smithsonian Institution
Astrophysical Observatory
Cambridge, Massachusetts 02138

The Smithsonian Astrophysical Observatory
is a member of the
Harvard-Smithsonian Center for Astrophysics

COSMOLOGICAL IMPLICATIONS OF *ROSAT* OBSERVATIONS OF GROUPS AND CLUSTERS OF GALAXIES

LAURENCE P. DAVID, CHRISTINE JONES, AND WILLIAM FORMAN
Smithsonian Astrophysical Observatory, Harvard-Smithsonian Center for Astrophysics, 60 Garden Street, Cambridge, MA 02138

ABSTRACT

We have combined *ROSAT* PSPC and optical observations of a sample of groups and clusters of galaxies to determine the fundamental parameters of these systems (e.g., the dark matter distribution, gas mass fraction, baryon mass fraction, mass-to-light ratio, and the ratio of total-to-luminous mass). Imaging X-ray spectroscopy of groups and clusters show that the gas is essentially isothermal beyond the central region, indicating that the total mass density (mostly dark matter) scales as $\rho_{dark} \propto r^{-2}$. The density profile of the hot X-ray–emitting gas is fairly flat in groups with $\rho_{gas} \propto r^{-1.0}$ and becomes progressively steeper in hotter richer systems, with $\rho_{gas} \propto r^{-2.0}$ in the richest clusters. These results show, that in general, the hot X-ray–emitting gas is the most extended mass component in groups and clusters, the galaxies are the most centrally concentrated component, and the dark matter is intermediate between the two. The flatter density profile of the hot gas compared to the dark matter produces a gas mass fraction that increases with radius within each object. There is also a clear trend of increasing gas mass fraction (from 2% to 30%) between elliptical galaxies and rich clusters due to the greater detectable extent of the X-ray emission in richer systems. For the few systems in which the X-ray emission can be traced to the virial radius (where the overdensity $\delta \approx 200$), the gas mass fraction (essentially the baryon mass fraction) approaches a roughly constant value of 30%, suggesting that this is the true primordial value. Based on standard big bang nucleosynthesis, the large baryon mass fraction implies that $\Omega = 0.1$–0.2. The antibiased gas distribution suggests that feedback from galaxy formation and hydrodynamics play important roles in the formation of structure on the scale of galaxies to rich clusters.

All the groups and clusters in our sample have mass-to-light ratios of $M/L_V \sim 100$–$150\ M_\odot/L_\odot$, which strongly contrasts with the traditional view that the mass-to-light ratio of rich clusters is significantly greater than individual galaxies or groups with $M/L_V \sim 250$–$300\ M_\odot/L_\odot$. We also show that M/L_V is essentially constant within the virial radius of clusters (where $\delta \gtrsim 200$), which is consistent with the peaks formalism of biased galaxy formation. While the mass-to-light ratios of groups and clusters are comparable (indicating a constant mass fraction of optically luminous material), the ratio of the total mass-to-luminous mass (gas plus stars) monotonically decreases between galaxies and clusters. The decrease in M_{tot}/M_{lum} arises from two factors: (1) the composition of baryonic matter varies from a predominance of optically luminous material (stars) on the scale of galaxies (~ 10 kpc) to a predominance of X-ray luminous material (hot gas) on the scale of rich clusters (~ 1 Mpc), and (2) the hot gas has a more extended spatial distribution than the gravitating matter. The observed *decrease* in M_{tot}/M_{lum} between galaxies and clusters indicates that the universe actually becomes "brighter" on mass scales between 10^{12} and $10^{15}\ M_\odot$, in the sense that a greater fraction of the gravitating mass is observable.

Subject headings: cosmology: theory — galaxies: clusters: general — galaxies: fundamental parameters — X-rays: galaxies

1. INTRODUCTION

One of the primary objectives of observational cosmology is to determine the distribution of luminous and dark matter in the universe. Historically, the search for luminous matter has primarily been restricted to the fairly narrow optical region of the spectrum. As new spectral windows have opened to astronomers over the past few decades, some of the previously termed "dark" matter has been found to emit profusely in other portions of the spectrum. A prime example is that in rich clusters of galaxies. Recent X-ray observations have shown that approximately 30% of the total gravitating mass in rich clusters resides in hot X-ray–emitting gas (Briel, Henry, & Bohringer 1992; Elbaz, Arnaud, & Bohringer 1994; Daines 1994). The presence of hot gas in hydrostatic equilibrium in elliptical galaxies, groups, and clusters (e.g., Jones & Forman 1984; Forman, Jones, & Tucker 1985; Sarazin 1986; Fabian, Nulsen,

& Canizares 1991) makes X-ray astronomy an ideal tool for probing the distribution of luminous and dark mass on the scales of galaxies to rich clusters. Such information places strong constraints on theories of galaxy formation, cluster formation, and cosmological scenarios governing the formation of structure in the universe.

Until recently, most estimates on the total gravitating mass in clusters were based on the distribution of galaxy redshifts. Several different methods have been developed and include: the virial mass estimator, the projected mass, the median mass estimator, and the average mass estimator (Heisler, Tremaine, & Bahcall 1985). The virial mass estimator is the most commonly used method and is based on a number of assumptions, which include virial equilibrium, mass follows the light, and an isotropic velocity dispersion (Binney & Tremaine 1987). Fundamentally, all mass estimates based on galaxy redshifts are

model dependent since the mass depends on the tangential component of the velocity dispersion which is unobservable. Even for the Coma cluster, for which a wealth of optical data is available, including almost 300 redshifts, Merritt (1987) and The & White (1986) have shown that by relaxing the mass-follows-light assumption, models with masses that differ by an order of magnitude are fully consistent with the data. The optical data alone cannot distinguish between low-mass models with radially decreasing mass-to-light ratios having predominantly circular orbits, or high-mass models with radially increasing mass-to-light ratios having predominantly radial orbits.

X-ray observations have several advantages over optical observations for determining the total mass in groups and clusters. Since the electron mean free path of the hot gas in a cluster is much less than the scale length of the X-ray emission and the sound crossing time is less than the dynamical time, the cas can be treated as a fluid in hydrostatic equilibrium. Under these circumstances, the gravitating mass of a cluster can then be determined directly from the gas density and temperature profiles, both of which are observable. The primary difficulty in determining the binding mass of clusters from X-ray missions prior to *ROSAT* was the lack of spatially resolved X-ray spectra, required to determine the temperature profile of the gas. Usually only one global temperature estimate was available. Previous methods typically assumed a certain parametric form for the temperature distribution, such as isothermal (Jones & Forman 1984) or polytropic (Cowie, Henriksen, & Mushotzky 1987). Hughes (1989) has shown that once a certain parameterization for the temperature profile is assumed, however, that the resulting range of acceptable gravitating masses is strongly limited. The *ROSAT* PSPC with its combined spatial and spectral resolution is an ideal instrument for studying groups and cool ($kT \sim 1\text{--}3$ keV) clusters. The gas temperature distribution is now known for several elliptical galaxies, groups, and cool clusters from *ROSAT* PSPC observations (Ponman & Bertram 1993; Forman et al. 1993; Jones et al. 1994; Trinchieri et al. 1994; David et al. 1994b; David, Forman, & Jones 1994a). Over the next decade the number of hotter clusters with measured temperature profiles will increase dramatically with observations by *ASCA, Spectrum X-Gamma, XMM,* and *AXAF*.

A traditional parameterization of the amount of dark matter on different scales is the mass-to-light ratio (see Tremaine 1992 for a recent review). Typical mass-to-light ratios are 3 $M_\odot/L_\odot$ in the solar neighborhood, 10 $M_\odot/L_\odot$ in the luminous portions of galaxies, and 100 $M_\odot/L_\odot$ for the total mass in a galaxy. Estimates of the gravitating mass in clusters based on the distribution of galaxy redshifts typically give $M/L \sim$ 300 $M_\odot/L_\odot$. This increase in M/L with mass scale is usually interpreted as evidence that there is a greater fraction of dark matter on large scales. All of these estimates for M/L fall far short of that required if the mass density of the universe is equal to the critical density ($M/L \approx 1000 \, M_\odot/L_\odot$). The common assumption to reconcile this discrepancy with an Einstein–de Sitter universe is that galaxy formation is biased to regions with high initial overdensities, such as proto-groups or clusters (Davis et al. 1985; Bardeen et al. 1986). Blumenthal et al. (1984) showed that while the M/L increases between galaxies and clusters, the more physically meaningful ratio of total mass-to-luminous mass (hot gas plus stars), M_{tot}/M_{lum}, remains roughly constant. This is due to the different stellar populations in early-type galaxies which dominate the cores of rich

clusters, and the inclusion of the gas mass (taken as 10% of the total mass). While a gas mass fraction of 10% is appropriate for the cores of rich clusters, the more sensitive *ROSAT* images have shown that the gas mass fraction increases up to 30% at large radii since the hot gas is the most extended component in rich clusters (Briel et al. 1992; Elbaz et al. 1994; Daines 1994). We will show that once these larger values for the gas mass fraction are taken into account, M_{tot}/M_{lum} *decreases* significantly as the scale increases from galaxies to rich clusters.

The large baryon mass fraction in rich clusters is inconsistent with standard big bang nucleosynthesis calculations (Walker et al. 1991) if $\Omega = 1$, as noted by White (1992). The primary uncertainty involved in this comparison is whether the presently observed gas mass fraction in rich clusters is a true reflection of the primordial value. Most cosmological scenarios assume that the presently observed structure in the universe developed solely by gravitational instability. If this were true, then the gas distribution should follow the total mass distribution, which is inconsistent with X-ray observations. Instead, the gas to total mass fraction monotonically increases from 2% to 30% on scales between 100 kpc and 1 Mpc and then remains roughly constant up to the largest scales surveyed in our cluster sample (~ 4 Mpc). This strongly suggests that the primordial baryon mass fraction is approximately 30% and the distribution of gas has been significantly altered by hydrodynamics on scales less than 1 Mpc, possibly due to feedback during galaxy formation.

This paper is organized in the following manner. Section 2 contains a description of the *ROSAT* PSPC data analysis. The PSPC observations of several objects in our sample already have been presented in the literature, and we compare our results in § 3. The main results are presented in § 4 (mass-to-light ratio), § 5 (gas mass fraction), and § 6 (ratio of total mass-to-luminous mass). The cosmological implications of our observations are discussed in § 7, and a brief summary of our main results are given in § 8.

2. DATA REDUCTION

To determine how the luminous (gas and galaxies) and dark components of the mass vary between galaxies, groups, and clusters, we compiled a sample of these objects that were observed by the *ROSAT* PSPC and satisfy a number of selection criteria (see Table 1). All of the objects in our sample have high X-ray fluxes based on the catalog in David et al. (1993), exhibit circularly symmetric X-ray emission (which greatly simplifies the mass determination), and span a range of gas temperatures and luminosities. The optical criteria include either the availability of photometric data to determine the total optical light, galaxy redshifts, or preferably both.

The prevalence of diffuse X-ray–emitting gas in groups is not well understood at present, but appears to be more common in dense elliptical-dominated systems. Such systems are not as abundant as loose spiral-dominated groups, most of which are probably not yet virialized. The observed trends we report on the gas mass fraction, baryon fraction, and ratio of total to luminous mass are derived from dense elliptical-dominated systems. In such dense systems, the presently observed X-ray–emitting gas consists of both primordial gas (residual gas remaining after the epoch of galaxy formation that was shock heated to the virial temperature of the group during its collapse) and gas injected from galactic winds. In the more common loose spiral-dominated groups, any residual gas

TABLE 1
SAMPLE PARAMETERS

Name	Class or N_A	kT (keV)	R_{20} (Mpc)	β	p	σ_p (km s^{-1})
NGC 4636	E	0.73 [0.71–0.75]ᵃ	0.10	0.53 [0.51–0.56]	...	...
NGC 2300	G	0.85 [0.73–0.96]ᵇ	0.20	0.40 [0.37–0.44]	...	...
HCG 62	G	0.93 [0.88–1.03]	0.50	0.38 [0.33–0.42]	0.15 [0.12–0.18]	...
NGC 5044	G	0.98 [0.96–1.00]	0.40	0.53 [0.51–0.55]	0.13 [0.10–0.16]	...
A539	50	1.3 [1.0–2.1]	1.2	0.65 [0.62–0.68]	0.24 [0.03–0.41]	793 [735–867]
A262	40	1.4 [1.2–1.5]	1.3	0.53 [0.50–0.56]	0.02 [−0.10–0.15]	498 [448–569]
A2589	40	3.0 [2.4–3.9]	2.0	0.57 [0.54–0.60]	...	918 [822–1057]
A2063	63	4.1 [3.3–5.3]	1.2	0.67 [0.63–0.71]	...	549 [497–621]
A1795	115	5.3 [5.2–5.4]	2.2	0.74 [0.72–0.75]	...	789 [714–894]
A85	59	6.2 [5.7–6.6]	3.1	0.62 [0.60–0.65]	...	993 [844–1260]ᶜ
A2029	82	7.8 [6.8–9.2]	2.9	0.65 [0.63–0.68]	...	...

NOTES.—This table lists the objects in our sample with their classification (E: elliptical, G: group, and the Abell number N_A for the clusters); the emission-weighted gas temperatures [determined from PSPC data for the groups and cool clusters and from MPC (A2063, A85, A2029) and Ginga (A1795) data for the hot clusters]; the radius at which the net X-ray surface brightness decreases to 20% of the 0.5–2.0 keV sky background, R_{20}; the best-fit β; the best-fit slope of the power-law temperature profile, ($T \propto r^{-p}$); and line-of-sight galaxy velocity dispersion. Errors are given at the 90% confidence limit for one interesting free parameter ($\chi^2_{\min} + 2.7$), except for σ_p for which the 68% errors are given.

ᵃ Only data between 2′ and 8′ are used in the spectral analysis.
ᵇ N_H is fixed to the galactic value in the spectral analysis.
ᶜ Line-of-sight velocity dispersion excluding the low-redshift group.

remaining after the initial epoch of galaxy formation was never shock heated to X-ray-emitting temperatures and may now reside in extended H I disks around the spiral galaxies.

2.1. Spatial Analysis

The X-ray emission from gas with $kT \gtrsim 1$ keV is significantly harder than the X-ray background in the ROSAT PSPC energy range. Thus, by restricting the spatial analysis to photons detected within the four highest energy bands (roughly 0.5–2.0 keV) defined by Snowden et al. (1994), we can significantly improve the sensitivity of the PSPC observations. The energy-screened PSPC images are flattened (corrected for nonuniform exposure and vignetting) by generating the four energy-dependent PSPC exposure maps and applying them to the images. The emission from point sources is excised using circular regions centered on each source with a 1′ radius for nearly on-axis sources. The radius of the circular region increases with off-axis angle according to the prescription for the PSPC PSF given by Hasinger et al. (1994). Surface brightness profiles for the diffuse emission are generated by extracting the data in concentric 30″ annuli. The surface brightness profiles are then fitted to a function of the form given by the standard hydrostatic-isothermal β model (Cavaliere & Fusco-Femiano 1976)

$$\Sigma(b) = \Sigma_0 \left[1 + \left(\frac{b}{a}\right)^2 \right]^{-3\beta + 1/2} \tag{1}$$

with the addition of a flat background component. The models are first convolved with the spatially dependent 1 keV PSPC point spread function, and fit to the data with a, β, and the background normalization treated as free parameters. The minimum χ^2 is significantly reduced by excluding the data within the central cooling regions. Systematic errors in the exposure maps produce a 10%–20% increase in the background surface brightness beyond 50′ off-axis, and this region also is excluded from the fitting procedure. The best-fit model parameters are listed in Table 1 for 11 galaxies, groups, and clusters.

For isothermal gas, the observed surface brightness is a direct measure of the emission integral along the line of sight and the gas density is given by

$$\rho_{\rm gas}(r) = \rho_0 \left[1 + \left(\frac{r}{a}\right)^2 \right]^{-3\beta/2} . \tag{2}$$

Our spectral analysis presented below and the results of other investigations on the temperature profile in ellipticals, groups, and cool clusters (Ponman & Bertram 1993; Forman et al. 1993; Jones et al. 1994; Trinchieri et al. 1994; David et al. 1994a, b; Daines 1994) show that the gas is essentially isothermal beyond the central cooling flow region. In particular, David et al. (1994b) showed that the gradual decrease in the gas temperature observed in the NGC 5044 group ($T \propto r^{-0.13}$) only produces a 10% variation in the fraction of the bolometric luminosity emitted within the PSPC energy band. Therefore, equation (2) provides a very accurate description of the gas density distribution.

The normalization of the density distribution ρ_0 is determined by equating the observed X-ray luminosity with the luminosity computed from the best-fit β and spectral models (including the temperature and abundance of the hot gas). For the hot clusters ($kT \gtrsim 3$ keV), we use an abundance of 30% solar based on Ginga observations (Hatsukade 1989). The exact abundance of heavy elements in hot clusters has little effect on ρ_0 since most of the X-ray emission arises from thermal bremsstrahlung. For the cooler clusters and groups, we use the best-fit abundance derived from spectral analysis of the PSPC data. At present, there is some discrepancy between ROSAT PSPC and ASCA SIS results concerning the abundance of the hot gas in groups. For example, the PSPC data on the NGC 5044 group give a best-fit abundance of 80% solar (David et al. 1994b) compared to 25% obtained from the SIS data (Mushotzky 1994). The SIS data also require excess absorption above the galactic value, while the PSPC data are consistent with galactic absorption. However, there are still important calibration issues to be resolved with ASCA which will have a significant impact on the spectral analysis of extended sources (Takahashi et al. 1994). Even if we assume the

low SIS abundance for the NGC 5044 group, the gas mass only increases by 30% and the baryon mass (gas plus stars) by 15%. Since this is much less than the observed factor of 3 increase in the baryon mass fraction between groups and rich clusters (see below), the exact abundance used for the groups does not have any affect on the main conclusions of our paper. We use $H_0 = 50$ km s^{-1} Mpc^{-1} throughout the paper.

2.2. *Spectral Analysis*

To determine the gravitating mass in a group or cluster, both the gas density and temperature profiles must be known. Due to the cutoff in the effective area of the *ROSAT* mirrors above 2.4 keV, the PSPC is best suited to determine the temperature profile in groups and relatively cool clusters. Of the seven objects in our sample with $kT < 3$ keV (see Table 1), only the NGC 2300 group has an insufficient number of detected photons to perform spatially resolved spectroscopy. For the remaining six objects, source spectra were extracted in concentric annuli in each object with widths ranging from 2' to 6' (depending on the photon statistics) within a radius of 16'. Background spectra were extracted from annuli between 30' and 45' off-axis, depending on the extent of the source emission. Charged particles were removed from the background and source spectra using the average master veto rates during the observations and the algorithms in Plucinsky et al. (1993). The charged particle subtracted background spectra were then adjusted for the differential vignetting of the *ROSAT* mirrors, before the background spectra were subtracted from the source spectra. The net spectra in PI channels 5 to 30 (in the 34 channel binning scheme) are then fitted to Raymond thermal plasma models with the galactic N_H, gas temperature, and abundance of heavy elements treated as free parameters.

A common feature in all of the temperature profiles is the presence of cooler gas in the central regions (see Ponman & Bertram 1993; Trinchieri et al. 1994; David et al. 1994a, b, for a detailed discussion of the temperature profiles in these systems). To determine the true (deprojected) gas temperature profiles beyond the central cooling flow regions, we generated cluster models in which the emission was divided into several concentric shells (with radii that correspond to the extracted spectra). A power-law profile is assumed for the temperature distribution ($T \propto r^{-p}$) and the abundance of heavy elements ($Z \propto r^{-q}$). Spectral models are generated by integrating the emission along the line of sight and folding the projected spectra through the *ROSAT*/PSPC instrument response. The models are then simultaneously fitted to all the extracted spectra beyond the cooling flow region. The free parameters include the normalization of the temperature profile, its slope p, the gas density in each shell, the normalization of the abundance profile, and its slope q. The best-fit power-law index for the temperature profile p and its uncertainty are given in Table 1. The distribution of heavy elements can only be tightly constrained for the NGC 5044 group, and the results are given in David et al. (1994b).

2.3. *Gravitating Mass Distribution*

Once the gas density and temperature profiles have been determined, the distribution of total gravitating mass can be calculated from the equation of hydrostatic equilibrium

$$M_{tot}(<r) = -\frac{kTr}{\mu m_p G}\left(\frac{d\ln\rho_{gas}}{d\ln r} + \frac{d\ln T}{d\ln r}\right), \qquad (3)$$

where the symbols have the usual notation. For the groups and cool clusters in our sample, the gravitating mass is determined from the best-fit β model (which gives the density distribution of the gas), and the best-fit power-law temperature profile. The gravitating mass in the elliptical NGC 4636, the NGC 2300 group, and the hotter clusters are determined by assuming an isothermal profile. The spectral analysis of NGC 4636 by Trinchieri et al. (1994) showed that, between 10 and 40 kpc, the gas is nearly isothermal. From the results in David et al. (1994a, b) on the NGC 5044 group, A262, and A539, estimates on the gravitating mass assuming the gas is isothermal only underestimate the mass (due to the central cooling flows) by 10%, 5%, and 3%, respectively, relative to the mass derived from the best-fit power-law temperature profile.

While the PSPC is best at determining the temperature profile in cooler systems it can still be used to place significant constraints on hotter clusters. Henry, Briel, & Nulsen (1993) have shown that the temperature profile in A2256 ($kT \approx 7$ keV) is consistent with an isothermal distribution and demonstrated the accuracy of the PSPC compared to previous non-imaging detectors sensitive to harder X-rays. Daines (1994) extracted spectra in several concentric annuli in A2029 ($kT \approx 8$ keV) and A85 ($kT \approx 6$ keV) and found that the best-fit temperatures in each annulus were equal within the errors (approximately 20%). Hughes (1989) combined X-ray data on the Coma cluster from *Ginga*, *Tenma*, and four pointed *EXOSAT* observations. All these instruments have different fields of view and can be used to constrain the gas temperature profile. If we use $\beta = 0.76$ and assume that the gas is isothermal ($kT = 8.3$ keV), we obtain a total gravitating mass within 1 Mpc that is only 16% greater than the best-fit mass-follows-light model in Hughes. This exercise shows that even for systems as hot as the Coma cluster, the isothermal assumption gives quite accurate mass estimates.

We do not attempt to determine the gravitating mass at small radii due to the presence of cool gas. To determine the gravitating mass within a cooling flow, the temperature of the ambient gas (which is required in the equation of hydrostatic equilibrium) must be known. The ambient gas temperature cannot be tightly constrained with the PSPC data due to its moderate spectral resolution. We therefore only calculate the distribution of gravitating mass beyond the cooling flow region and within the radius where the net X-ray surface brightness exceeds 20% of the sky background (see Table 1).

3. COMPARISON WITH PREVIOUS *ROSAT* RESULTS

The PSPC observation of the elliptical galaxy NGC 4636 was previously discussed by Trinchieri et al. (1994). They found that the surface brightness profile flattens slightly beyond 8' from the center of the galaxy, possibly due to diffuse emission from the Virgo cluster. They also found that the spectrum of NGC 4636 could be fitted equally well with either a two-temperature model (each with solar abundances) or a single-temperature Raymond model with an abundance of only 20% solar. Since we are interested in the properties of a typical elliptical galaxy, we have restricted our analysis to the central 8' (40 kpc). Our spatial and spectral analysis are fully consistent with the results in Trinchieri et al. (1994). Fitting the observed 0.5–2.4 keV surface brightness profile to a β model we obtain the best fit with $\beta = 0.50 \pm 0.02$, while the core is unresolved. The temperature in the central 2' (10 kpc) is less than the surrounding gas temperature, suggesting the presence of a cooling flow. Fitting the emission between 2' and 8' to a

single-temperature Raymond model, we obtain a best fit with $kT = 0.73 \pm 0.02$ keV, $Z = 0.30 \pm 0.06$ (with $Fe_\odot/H_\odot = 4.68 \times 10^{-5}$), and $N_H = 1.4 \times 10^{20}$ cm^{-2} (consistent with the galactic value). The spatially resolved spectral analysis in Trinchieri et al. shows that the gas temperature between 2' and 8' is consistent with an isothermal distribution.

Our analysis of HCG 62 is in complete agreement with the initial analysis by Ponman & Bertram (1993). The X-ray emission from this group can be traced to a projected distance of 400 kpc, and the surface brightness profile is best fitted with $\beta = 0.38 \pm 0.04$. Fitting a Raymond thermal plasma model to the integrated emission from the group we obtain a best fit with $kT = 0.93 \pm 0.03$ keV. Due to the large number of net counts in this observation, we are able to extract spectra in four annuli beyond the central cooling flow region. The deprojected temperature profile is best fitted with a power-law index of $p = 0.15 \pm 0.03$.

The only object in our sample for which our analysis differs from previous work is the NGC 2300 group (Mulchaey et al. 1993). Using the total gravitating mass in the note added in proof gives a ratio of total to luminous mass of approximately 16. A recent analysis by Henriksen & Mamon (1994) based on the X-ray surface brightness profile published in Mulchaey et al. suggests that the baryon fraction was initially underestimated by a factor of 4–5. Our analysis of the PSPC observation shows that the surface brightness profile of the NGC 2300 group is best fitted with $\beta = 0.40 \pm 0.05$ (similar to other groups observed by ROSAT and Einstein) and that the temperature of the diffuse gas is 0.85 keV. Since there are an insufficient number of detected photons to determine the temperature profile we assume, as did Mulchaey et al., that the

gas is isothermal. The net X-ray surface brightness of the NGC 2300 group drops below 20% of the sky background at a projected radius of approximately 200 kpc. We derive a total gravitating mass of 7.6×10^{12} $M_\odot$ within this radius. Mulchaey et al. give a total mass of 2×10^{13} $M_\odot$ within 300 kpc in their note added in proof, which corresponds to a total mass of 1.3×10^{13} $M_\odot$ within 200 kpc. Using the same mass-to-light ratios for the three brightest galaxies in the group as in Mulchaey et al., we find that $M_{tot}/M_{lum} = 8$–10 within 200 kpc in this group, which is consistent with other groups observed by the PSPC (see below).

4. MASS-TO-LIGHT RATIOS

Searching the literature we have obtained photometric observations for seven of the groups and clusters in our sample. The optical luminosity of the NGC 5044 group is determined from observations by Ferguson & Sandage (1990) who identified 162 member galaxies brighter than $m_B \sim 20$, with a completeness limit of $m_B \sim 18$. Melnick & Sargent (1977) list 45 galaxies brighter than $m_B \sim 16$ within 40' (1.1 Mpc) of the central dominant galaxy in A262. The total visual luminosity (V band) within 3 Mpc for the remaining clusters is obtained from Arnaud et al. (1992). The optical luminosities of the NGC 5044 group and A262 are corrected for incompleteness using a Schechter luminosity function and converted to V-band luminosities assuming $L_V = 1.3L_B$ (Faber & Gallagher 1979). We compute M/L_V within 250 kpc in the NGC 5044 group and within 1 Mpc in the clusters (see Fig. 1). The galaxy distribution in the clusters is determined using a modified King profile with the same core radius as the X-ray emission. The galaxy distribution in the NGC 5044 group is determined from
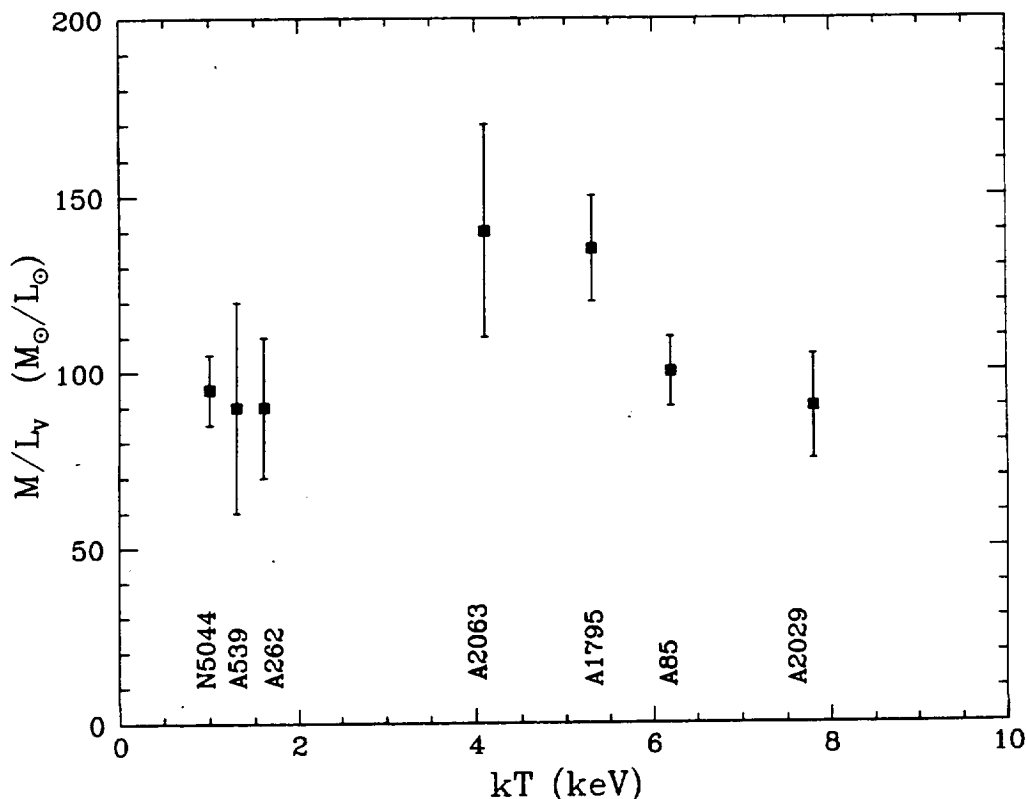

FIG. 1.—Mass-to-light ratios within 250 kpc for the NGC 5044 group and within 1 Mpc for the clusters. The error bars only reflect the uncertainties (at the 68% confidence limit) in the gravitating mass.

the best-fit King model to the observed galaxy distribution given by Ferguson & Sandage (1990).

4.1. *The Constant Value of* M/L_V *between Galaxies and Rich Clusters*

Our analysis shows that M/L_V is roughly constant between groups and rich clusters with $M/L_V \sim 100$–150 $M_\odot/L_\odot$ (see Fig. 1). This result indicates that the mass fraction of optically luminous material is roughly constant on scales of 10^{12} $M_\odot$ to 10^{15} $M_\odot$. Our result differs substantially from previous suggestions that M/L_V increases by a factor of 3 or more between galaxies and rich clusters, and that rich clusters typically have $M/L_V \sim 250$ $M_\odot/L_\odot$ (e.g., Faber & Gallagher 1979). Such high mass-to-light ratios arise from mass estimates based on the distribution of galaxy redshifts which are model dependent as discussed in the introduction, and are highly susceptible to substructure and superposition.

To compare the observed mass-to-light ratios with predictions of biased galaxy formation, we also plot the mass-to-light ratio as a function of the overdensity ($\delta = [\langle \rho \rangle - \rho_0]/\rho_0$) where $\langle \rho \rangle$ is the mean density within a given radius and ρ_0 is the critical density (see Fig. 2). Since we use a modified King profile for the galaxies, the galaxy light scales as $L \propto r^3$ within the core, and as $L \propto \ln r$ at large radii. Due to the observed isothermal gas temperature profiles which indicate that $M \propto r$, the mass-to-light ratio profiles decrease out to several core radii and then increase as $r/\ln r$ at large radii. The increase in M/L_V at small radii in the NGC 5044 group is due to the addition of the light from NGC 5044 itself, which comprises

approximately one-half of the total galaxy light from the group within 150 kpc. To directly compare the observed mass-to-light ratios with predictions of biased galaxy formation, M/L_V should be computed within the virial radius (where $\delta \approx 200$) in each object. Unfortunately, the X-ray emission can only be traced to this radius in A85 and A2029. There are, however, two other clusters (A539 and A262) in which the X-ray emission can be traced to $\delta \approx 400$. In general, Figure 2 shows that the observed values of M/L_V in our sample of groups and clusters are not very sensitive to δ for $\delta \lesssim 200$. This will be compared with expectations from biased galaxy formation in § 7.

4.2. *Comparison with Optical Data*

To investigate the difference between the cluster mass estimates derived from the X-ray and optical data, we obtained galaxy redshifts and positions for six clusters in our sample from the literature (A262: Moss & Dickens 1977, Zabludoff, Huchra, & Keller 1991; A539: Ostriker et al. 1988; A2589, A2063, A85: Beers et al. 1991; A1795: Hill et al. 1988). Using a program kindly provided to us by T. Beers, we computed the gravitating masses for the six clusters using the virial mass estimator (Binney & Tremaine 1987). Only galaxies within the central 3 Mpc of the clusters are included in our computation of the velocity dispersion, and the results are given in Table 1. For A539 we only include galaxies with velocities between 6500 and 10,500 km s^{-1} as in Ostriker et al. (1988). For A1795 we exclude the galaxies identified as nonmembers in Hill et al. (1988). A comparison of the cluster masses determined from the
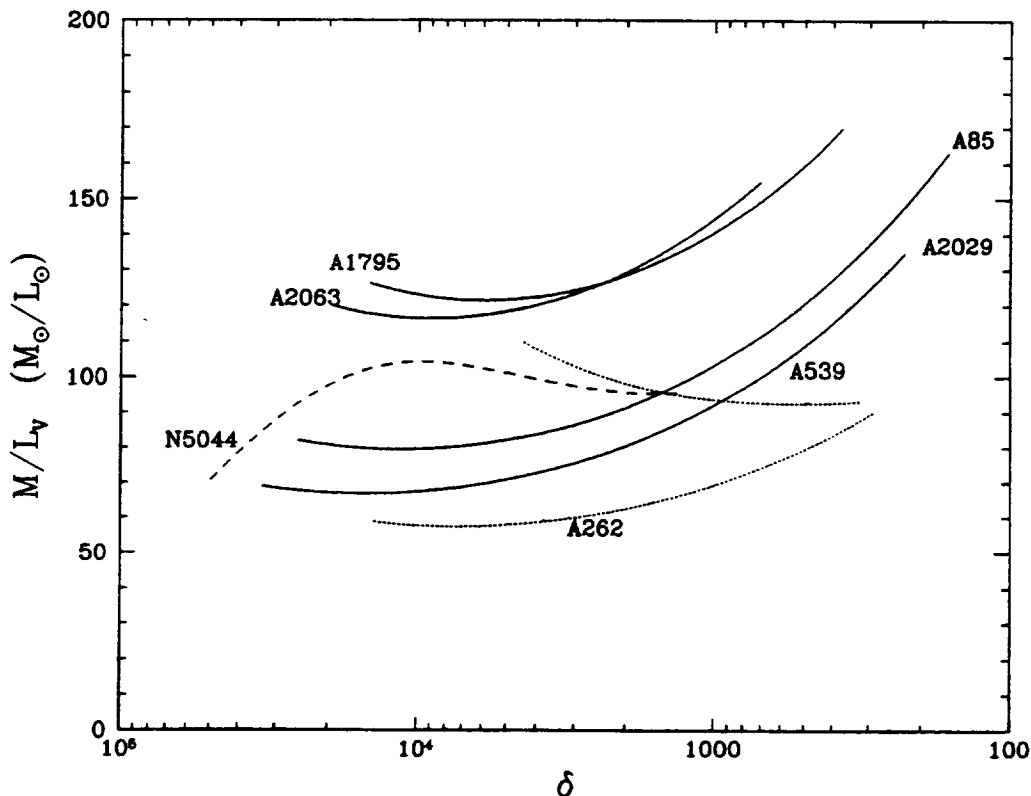

FIG. 2.—Mass-to-light ratios plotted as a function of the overdensity δ, within each object. The groups, cool clusters and hot clusters are plotted as dashed, dotted, and solid lines, respectively.

virial mass estimator and the equation of hydrostatic equilibrium is given in Figure 3. We also include A2029 in Figure 3 using the mass-to-light ratio of $M/L_V \sim 500\ M_\odot/L_\odot$ given in Dressler (1981), by simply scaling the mass using our value of $M/L_V = 90\ M_\odot/L_\odot$ (we use the same L_V as in Dressler). To determine the gravitating mass within 3 Mpc from the equation of hydrostatic equilibrium, we assume that the gas density and temperature profiles remain the same out to this radius. This assumption yields an upper limit on the true mass, since the gas temperature must eventually decline more rapidly for the gas to be gravitationally bound. Figure 3 shows that while there are a few clusters for which the two mass estimates are consistent, in general, there is a tendency to overestimate the gravitating masses using the optical data. The gravitating mass derived from the optical data overestimates the mass derived from the X-ray data more than a factor of 2, in three out of the seven clusters.

The three clusters with the largest discrepancy in the gravitating mass are A2029, A539, and A85. The velocity dispersion in A539 is very large ($\sigma_p = 793$ km s^{-1}) for a cool cluster. Virialized galaxies in A539 should have $\sigma_p \sim 400$ km s^{-1}, based on the gas temperature. Including all the galaxy redshifts in A85 gives a velocity dispersion of 1530 km s^{-1}. Beers et al. (1991) noted that there is evidence for a low-redshift group in A85. By removing the five lowest redshift galaxies, Beers et al. found that the virial mass decreased by a factor of 2.4. Excluding the same five galaxies as in Beers et al., we derive a virial mass for A85 in good agreement with results from the X-ray data (see Fig. 3). This example shows how the X-ray and optical data compliment one another in determining the galaxy dynamics in a cluster. Using various statistical tests to search for the presence of substructure, Bird, Dickey, & Salpeter (1993) and Davis et al. have shown that much of the discrepancy between optically and X-ray–determined cluster mass estimates can be reconciled once substructure is properly taken into account.

Faber & Dressler (1977) derived a velocity dispersion of 1514 km s^{-1} for A2029 based on 18 redshifts. However, by removing three galaxies in the sample, the velocity dispersion was reduced to 788 km s^{-1}. In a later paper, Dressler (1981) compiled 31 additional redshifts and obtained a velocity dispersion of 1430 km s^{-1}. Based on the observed gas temperature in this cluster, the velocity dispersion of virialized galaxies should be ~ 900 km s^{-1}, which is more consistent with the lower velocity dispersion for the 15 galaxies derived by Faber & Dressler (1977). The larger velocity dispersion obtained by Dressler (1981) suggests that there is significant substructure in A2029.

With the low-redshift group in A85 excluded, there are three clusters for which the optical and X-ray mass determinations are consistent (A2589, A1795, A85). In all of these cases, the galaxy redshifts are accumulated from within a few core radii of the central dominant galaxy. Large discrepancies in the two mass estimates are much more likely when the galaxy redshifts are accumulated over a broad region. This suggests that, in general, the central galaxies in clusters are virialized with isotropic velocity dispersions, while the outlying galaxies are either on predominantly radial orbits, or are just now falling
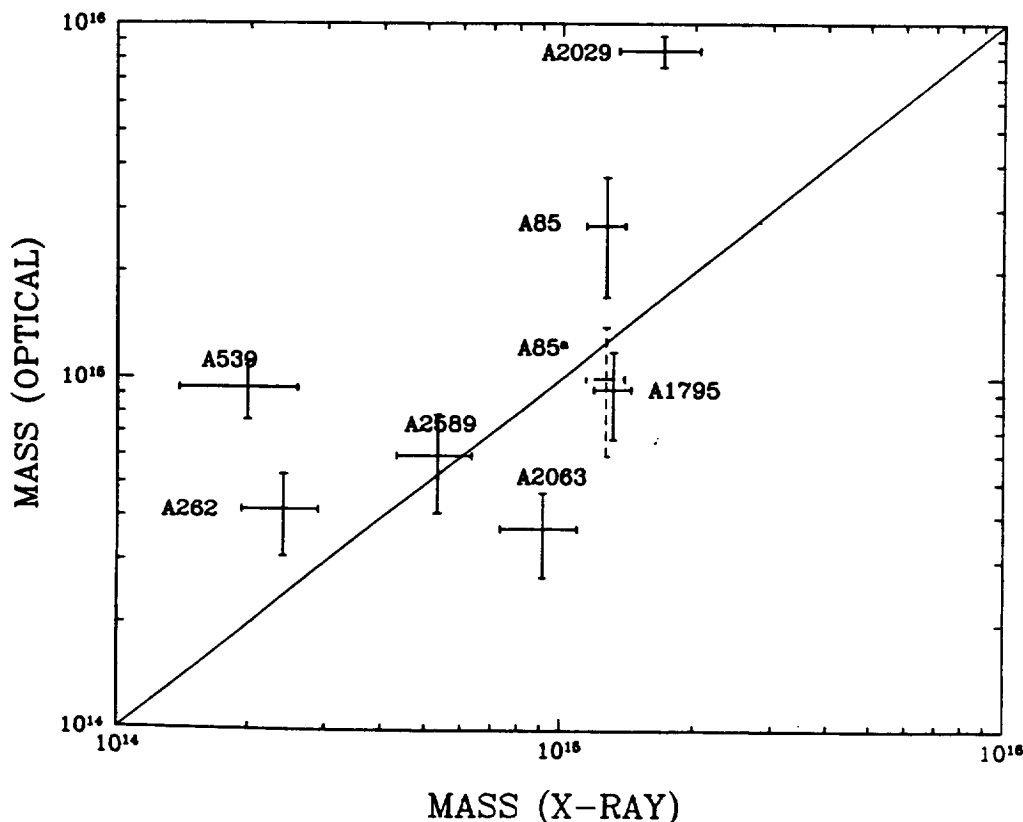

FIG. 3.—Comparison of the gravitating mass estimates for a sample of clusters determined from optical data (using the virial mass estimator) and X-ray data (using the equation of hydrostatic equilibrium). The dashed cross indicates the virial mass estimate of A85 excluding the low-redshift group of galaxies.

into the cluster for the first time. Such a situation is evident in the numerical simulations of Evrard (1990) in which the anisotropy parameter increases significantly with radius in clusters at the present time.

5. GAS MASS FRACTION

Since the extent of the X-ray emission differs significantly between galaxies, groups, and clusters (see Table 1) we compute the gas mass fraction, $f_{gas} = M_{gas}/M_{tot}$, as a function of encircled gravitating mass (or equivalently radius) in each object (see Fig. 4). For comparison with theoretical predictions we also plot f_{gas} as a function of the overdensity δ in each system in Figure 5. Estimates of f_{gas} in A2163 within two different radii also are included in Figures 4 and 5 from the analysis of the PSPC data presented in Elbaz et al. (1994). The rich cluster A2163 is the hottest ($kT \sim 14$ keV) and most X-ray luminous cluster known. The X-ray emission in A2163 can be traced to a record projected distance of 4.6 Mpc, corresponding to an encircled mass of $M_{tot} = 5 \times 10^{15}$ $M_{\odot}$ (Elbaz et al. 1994).

Our analysis shows that not only does f_{gas} increase with radius within each object, but that f_{gas} increases continuously between ellipticals, groups, and clusters. Figure 4 shows that the different overall gas mass fraction in these systems (2% in ellipticals, 10% in groups, 20%–30% in clusters) is primarily due to the greater extent to which the X-ray emission is detected in richer systems. In fact, Figure 4 shows that within a given encircled mass, the gas mass fraction is roughly independent of the richness of the system. For example, f_{gas} in the cores

of cool clusters is comparable to the overall value of f_{gas} in groups.

If cluster evolution were an entirely self-similar process, then f_{gas} should be a constant at a given overdensity in all objects. Figure 5 clearly shows that this is not the case, indicating that some additional physics has broken the self-similarity. Groups have a much lower gas mass fraction compared to rich clusters at the same overdensity. For example, at $\delta = 3000$, f_{gas} varies by a factor of approximately 7 between groups and clusters. In principle, all the objects should have the same value of f_{gas} at their virial radius (where $\delta = 200$). Mass shells with this overdensity should just now be collapsing onto these objects. The X-ray emission can only be traced to this radius in A85 and A2163. However, there are four other clusters in which the X-ray emission can be traced to a radius where δ approaches 400 (A262, A539, A1795, A2029). In all cases, f_{gas} appears to be approaching a common value between 25% and 30%. The only object which significantly departs from this trend is A2063. However, the X-ray emission can only be traced to a radius where $\delta \approx 700$, so it is difficult to extrapolate with confidence to the virial radius.

The variation of f_{gas} in our sample clearly shows that the hot gas is more uniformly distributed (antibiased) with respect to the underlying gravitating mass on scales between 10^{12} and 10^{15} $M_{\odot}$. If gravity were the only force governing the formation of structure on these scales (and the gas did not have an initial antibiasing), then the gas and total mass should have the same distribution. In order to generate a gas distribution which is antibiased with respect to the mass, reheating and
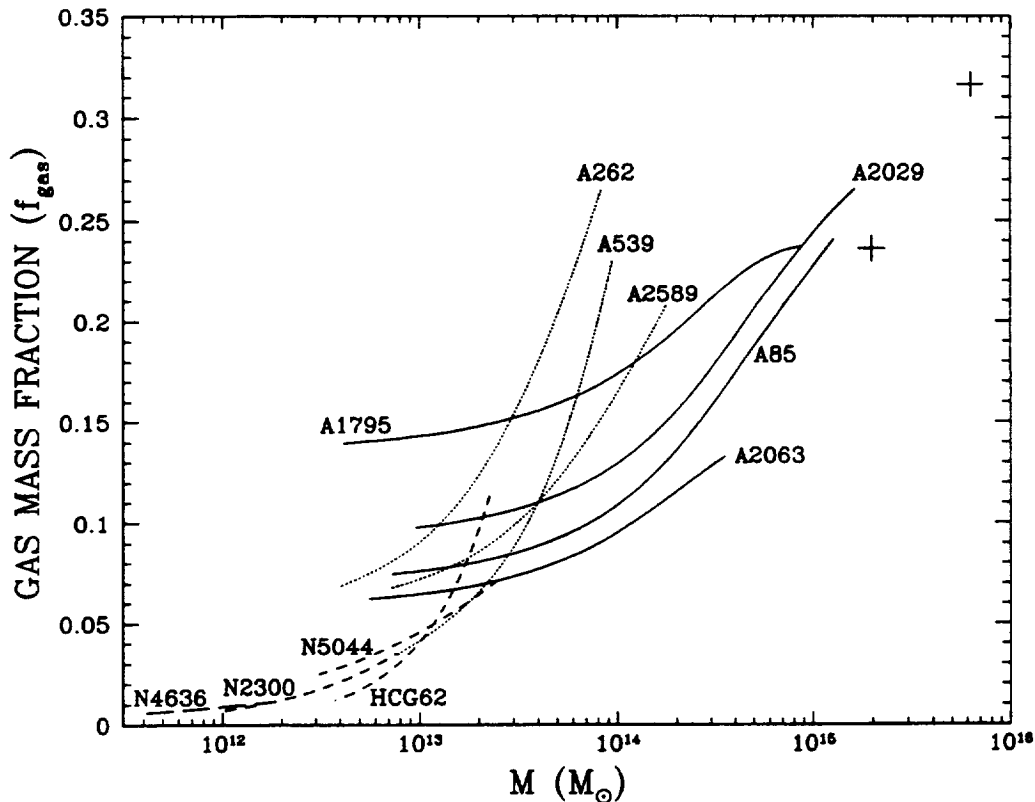
FIG. 4.—Gas mass fraction vs. encircled total gravitating mass for the entire sample. Ellipticals, groups, cool clusters, and hot clusters are plotted as long-dashed, short-dashed, dotted, and solid lines, respectively. The plus signs correspond to estimates on f_{gas} within two different radii in A2163.
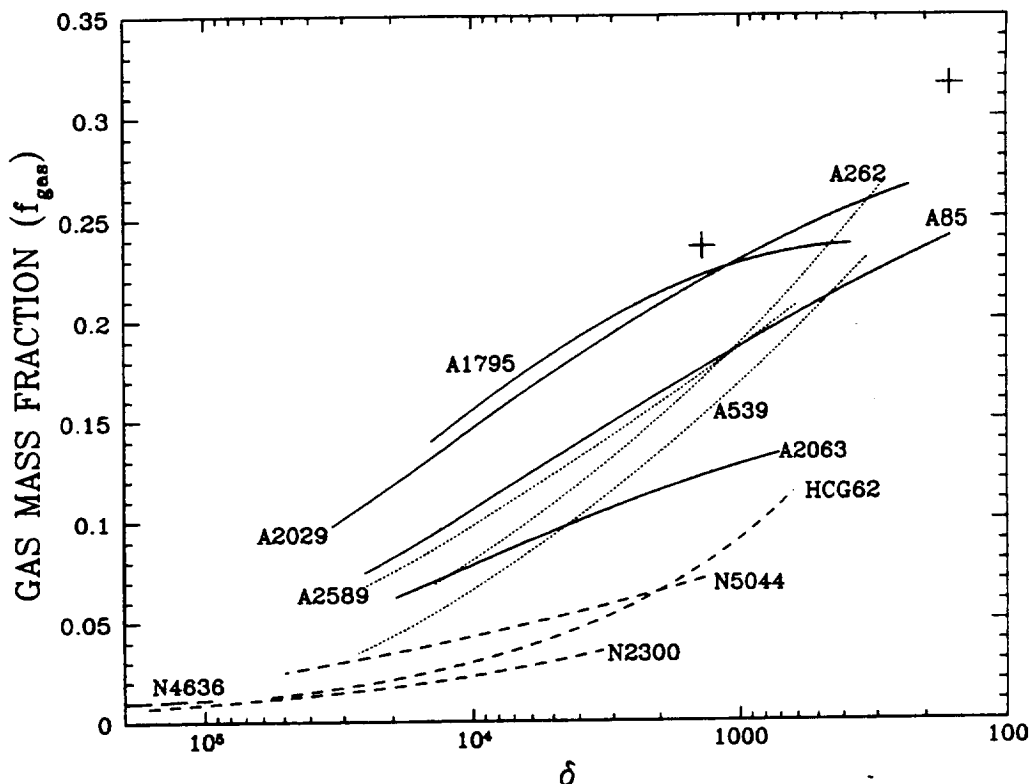
FIG. 5.—Gas mass fraction as a function of the overdensity δ, for each object in the sample. Line styles are the same as in Fig. 4. The plus signs correspond to estimates on f_{gas} within two radii in A2163.

hydrodynamics must play an important role in the formation of structure on these mass scales. This will be discussed in more detail in § 7.

6. RATIO OF MASS-TO-LUMINOUS MASS

The ratio of the total mass-to-luminous mass M_{tot}/M_{lum} is shown in Figure 6 for our sample of groups and clusters as a function of encircled gravitating mass. We define the luminous mass in clusters as the sum of the hot X-ray–emitting gas mass and the optically luminous mass in galaxies (determined using $M/L = 8\ M_\odot/L_\odot$). The ratio of total to luminous mass for the NGC 2300 group is only shown at a single radius since most of the optical luminosity arises from just three galaxies. We also have included M_{tot}/M_{lum} within two radii in A2163 from Elbaz et al. (1994). Figure 6 shows that M_{tot}/M_{lum} decreases rapidly between mass scales of 10^{12} and $10^{14}\ M_\odot$ and then becomes relatively constant on larger scales with $M_{tot}/M_{lum} \sim 3$. The rapid decrease in M_{tot}/M_{lum} between 10^{12} and $10^{14}\ M_\odot$ is primarily due to the increase in f_{gas} with radius (see Fig. 4). Figure 6 shows that by including the X-ray–emitting gas, a greater fraction of the total gravitating mass in rich clusters is observable compared to the fraction in groups and individual galaxies.

7. COSMOLOGICAL IMPLICATIONS

Prior to the use of X-ray observations as a tool for determining the gravitating masses of galaxies and clusters, it was generally accepted that M/L_V uniformly increased between galaxies, groups, and rich clusters with typical values for rich clusters being 300 $M_\odot/L_\odot$ (for reviews see Blumenthal et al. 1984 and

Tremaine 1992). Using imaging X-ray spectroscopy we have shown that the mass-to-light ratio of galaxies, groups, and clusters is approximately constant at 100–150 $M_\odot/L_\odot$. The uniformly distributed dark matter in clusters can simply result from the stripping of galaxy halos as clusters form through hierarchical merging as demonstrated in the simulations of Merritt (1984). Earlier reports of a continuous increase in M/L_V between galaxies and clusters was interpreted as evidence that the universe is "darker" on larger scales. X-ray observations have shown that a significant fraction of the gravitating mass in clusters (up to 6 times the mass in galaxies; David et al. 1990) is contained in the hot gas. Our analysis shows that the ratio of the total to luminous mass M_{tot}/M_{lum} monotonically decreases between galaxies and rich clusters. This indicates that the universe actually becomes "brighter" as mass scales increase from 10^{12} to $10^{15}\ M_\odot$.

Using nonimaging X-ray data from *HEAO 1*, Cowie et al. (1987) derived low mass-to-light ratios for a sample of clusters. The cluster mass estimates were based on the assumption of a polytropic equation of state for the gas. Four of the five clusters analyzed by Cowie et al. are strong cooling flow clusters with large amounts of cool gas in their cores. By fitting a single emission weighted X-ray spectrum with a radially decreasing temperature profile, they forced the central cool gas to lie in the outer regions of the clusters, and obtained fairly steep best-fit temperature profiles. The radially decreasing temperature profiles used to estimate the cluster masses in Cowie et al. are inconsistent with the observed isothermal temperature profiles obtained from imaging X-ray spectroscopy of *ROSAT* PSPC data.
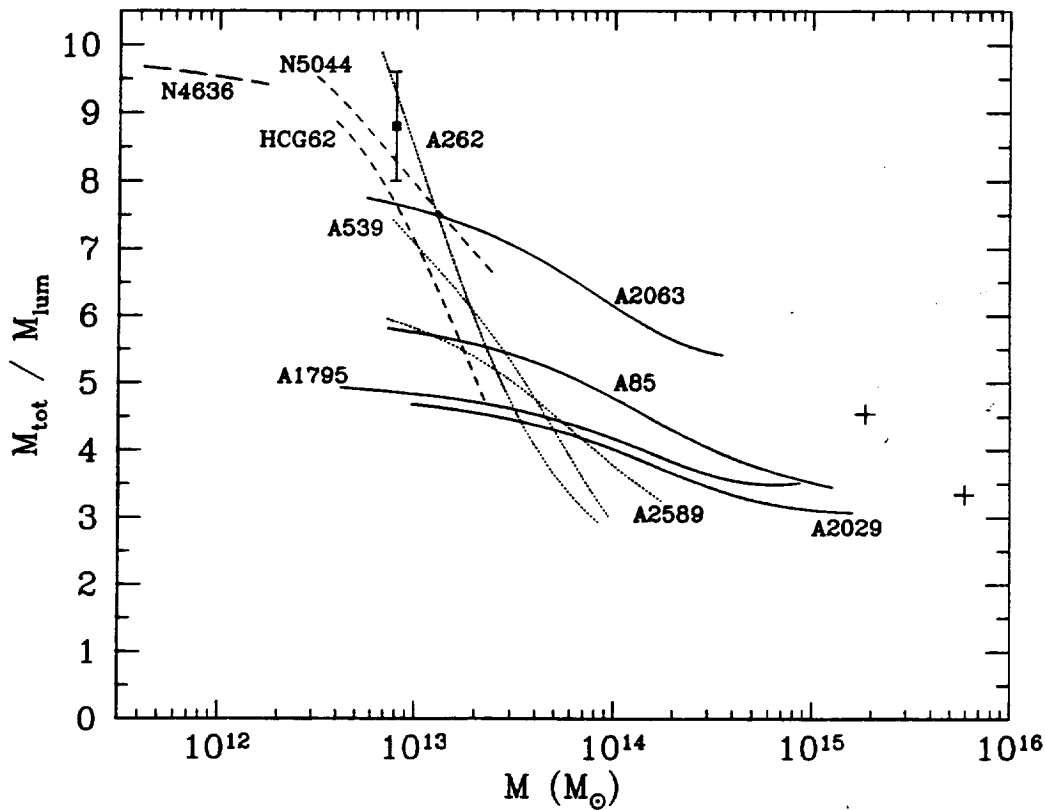
FIG. 6.—Ratio of total gravitating mass-to-luminous mass (gas plus stars) vs. the encircled total gravitating mass for the entire sample. The line styles are the same as in Fig. 4. The plus signs correspond to estimates of M_{tot}/M_{lum} within two radii in A2163.

7.1. *Is Galaxy Formation Biased?*

The basic premise in the peaks formalism of biased galaxy formation (Davis et al. 1985; Bardeen et al. 1986) is that galaxies only form at peaks in the primordial distribution of density fluctuations that exceed some critical density threshold. Assuming Gaussian random variables, the distribution of cluster and galaxy scale over densities can be described as a bivariate Gaussian in terms of the reduced parameters $v_c = \delta_c/\sigma_c$ and $v_g = \delta_g/\sigma_g$, where σ_c and σ_g represent the rms density fluctuations filtered on cluster and galactic scales, respectively (David & Blumenthal 1992). The joint distribution function is

$$f(v_g, v_c) = \frac{1}{2\pi\sqrt{1 - r^2}} \exp\left[-\frac{1}{2(1 - r^2)} (v_g^2 + v_c^2 - 2rv_c v_g)\right],$$

(4)

where the correlation coefficient is given by $r = \sigma_{gc}^2/(\sigma_c \sigma_g)$. The variances and correlation coefficient are determined by taking the proper moments of the power spectrum weighted by the appropriate filters

$$\sigma_{ij}^2 = \frac{V}{(2\pi)^6} \int d^3k \, |\delta_k|^2 W(kR_i)W(kR_j),$$

(5)

where $W(kR_j)$ is the top-hat window function. Assuming that only peaks filtered on a galaxy mass scale that exceed a global threshold of v_{th} develope into galaxies, the mass-to-light ratio of a cluster should be proportional to the total mass of a cluster divided by the mass within galaxy peaks with $v_g > v_{th}$. The mass fraction within a cluster scale fluctuation contained

within galaxy scale fluctuations that exceed the threshold for galaxy formation is given by the conditional probability

$$P(v_g > v_{th}\,|\,v_c) = \frac{1}{2}\,\mathrm{erfc}\left[\frac{v_{th} - rv_c}{\sqrt{2(1 - r^2)}}\right].$$

(6)

The condition for collapse of a density fluctuation at a redshift z, is given by $v_c(\mathrm{crit}) = 1.69(1 + z)/\sigma_c$. Assuming a power-law spectrum $(P \propto k^n)$, gives $r = (M_c/M_{gal})^{-(n + 3)/6}$, and $\sigma_c = (M_c/M_0)^{-(n + 3)/6}$, where M_c is the cluster mass, M_{gal} is a typical galaxy mass, and M_0 is some nominal mass scale (usually taken at $16 h_{50}^{-1}$ Mpc) at which the power spectrum is normalized. Substituting the expressions for r and σ_c into equation (6) gives

$$P[v_g > v_{th}\,|\,v_c = v_c(\mathrm{crit})]$$

$$= \frac{1}{2}\,\mathrm{erfc}\left[\frac{v_{th} - 1.69(1 + z)(M_0/M_{gal})^{-(n + 3)/6}}{\sqrt{2(1 - r^2)}}\right].$$

(7)

The only dependence on the cluster mass in this expression is given by the correlation coefficient in the denominator. The above expression for r shows that on cluster mass scales (many times the mass of individual galaxies), and for $n > -3$, that $r \to 0$ as M_c increases. Thus, the mass fraction within the virial radius of a cluster residing in galaxies is effectively independent of the cluster mass. This calculation shows that the near constant value of M/L_V in our sample of groups and clusters is consistent with the peaks formalism of biased galaxy formation. In the biased galaxy formation scenario, M/L_V should only increase significantly on mass scales where $\delta < 200$. As

lower density shells continue to collapse onto presently viria-lized objects, M/L_V will increase until, in an $\Omega = 1$ universe, the mass-to-light ratio of all virialized objects equals the value required for closure ($M/L_V \approx 1000$).

7.2. Constraints on Ω

The density of the universe cannot be inferred from the observed mass-to-light ratio of virialized objects without some prescription for galaxy formation. We can, however, constrain Ω using the observed baryon fraction (see White 1992). Standard big bang nucleosynthesis calculations (Walker et al. 1991) limit the baryonic component of the universe to

$$0.04 < \Omega_b h_{50}^2 < 0.06 , \qquad (8)$$

where $\Omega_b = f_b \Omega$, and f_b is the baryon mass fraction. In § 5, we showed that $f_{gas} \to 0.30 h_{50}^{-3/2}$ as $\delta \to 200$, indicating that the primordial baryon fraction is $\approx 0.30 h_{50}^{-3/2}$ (the addition of the mass in galaxies would only increase f_b by a small amount since the gas mass dominates the galaxy mass in rich clusters). Inserting the observed baryon fraction into equation (8) gives

$$0.13 h_{50}^{-1/2} < \Omega < 0.2 h_{50}^{-1/2} . \qquad (9)$$

The region in H_0 and Ω parameter space that satisfies the conditions given by equation (9) is illustrated in Figure 7. In addition, we also include the constraint that $f_b = 0.30 h_{50}^{-3/2} < 1$ (i.e., clusters cannot be more than 100% baryons). Figure 7 shows that if H_0 were very small, the observed baryon mass

fraction and big bang nucleosynthesis calculations would be consistent with a high-density universe ($\Omega > 0.3$). However, this would require clusters to be more than 100% baryons.

On much larger scales (~ 100 Mpc), an analysis of the QDOT IRAS galaxy redshift survey indicates that $0.6 < \Omega < 1.1$ (Kaiser et al. 1991). There are also indications on the scale of rich clusters that a high-density universe is required to account for the large fraction of clusters with observed sub-structure (Richstone, Loeb, & Turner 1992). Evrard et al. (1994) have performed numerical simulations of cluster forma-tion under a variety of cosmologies and find that simulations with $\Omega = 0.2$ (with or without a cosmological constant) produce more relaxed, spherically symmetric clusters than observed. The simulations in an $\Omega = 1$ universe, however, are based on a baryon mass fraction of only 10%. No simulations have yet been performed that simultaneously reproduce the observed frequency of substructure, the more extended gas distribution, and the high baryon fraction in rich clusters.

7.3. The Importance of Hydrodynamics for the Distribution of Baryons

The one common feature in most cosmological scenarios is that the observed structure in the universe results exclusively from gravitational instability. If gravity were the only force governing the growth of structure, than the baryons and dark matter should have similar distributions. One alternative to the gravitational instability scenario is a model in which early explosions sweep baryons into dense shells, leaving the dark matter relatively unperturbed (Ostriker & Cowie 1981). Clus-
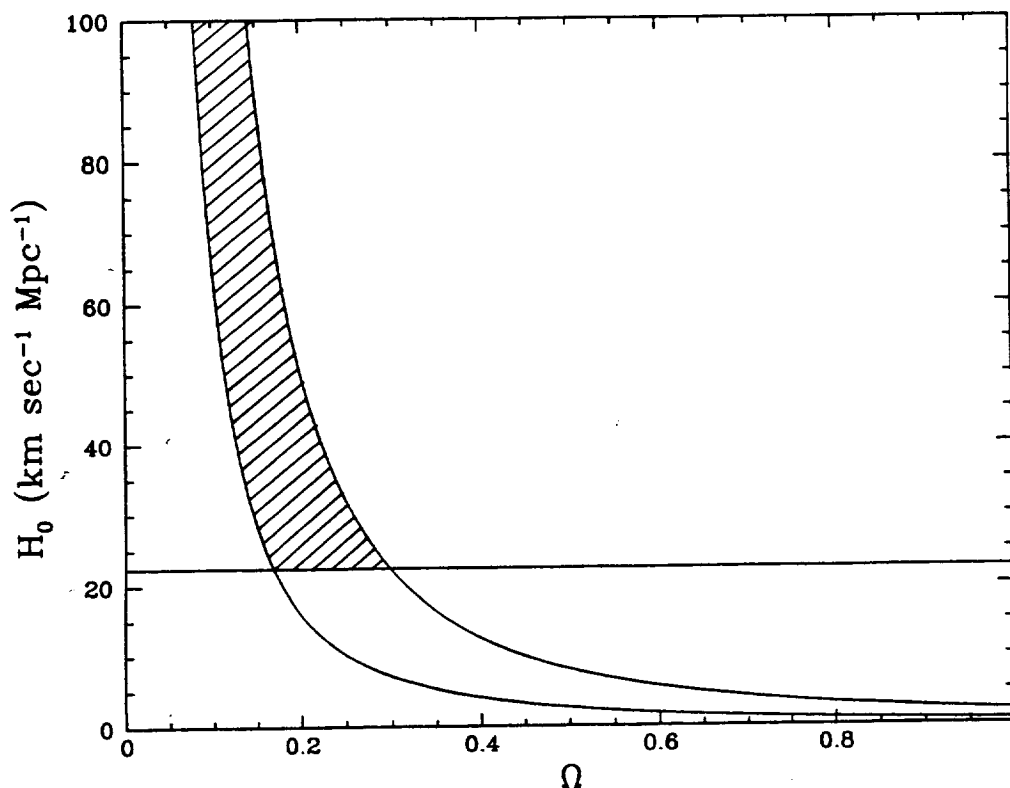

FIG. 7.—Permitted range in Ω and H_0 parameter space (shaded area) that satisfies both standard big bang nucleosynthesis calculations and the fact that clusters cannot be more than 100% baryons.

ters of galaxies are then assumed to form at the intersections of overlapping shells.

Feedback from galaxy formation can reheat the intergalactic medium through photoionization (due to the high abundance of massive stars and AGNs) and collisionally through galactic winds (driven by the high rate of Type II supernovae). While photoionization can only heat the gas up to $\sim 10^4$ K, heating by supernovae-driven galactic winds can heat the gas up to 10^8 K (David, Forman, & Jones 1991; White 1991). Heating by galactic winds can produce the observed flatter gas density distribution relative to the gravitating mass within individual clusters (White 1991; Metzler & Evrard 1994). Recent calculations have shown that galaxy feedback can have dramatic effects on the ionization and thermodynamic state of the intergalactic medium (Shapiro, Giroux, & Babul 1994; Cen & Ostriker 1994). The numerical simulations of large-scale structure presented by Cen & Ostriker show that galaxy feedback produces a hot intergalactic medium that is antibiased with respect to the gravitating mass, as is observed.

Early reheating of the gas in rich clusters has also been invoked by Kaiser (1991) to explain the observed negative X-ray luminosity evolution of rich clusters (a lower comoving number density of X-ray luminous clusters at $z \gtrsim 0.1$; Edge et al. 1990; Henry et al. 1992). Earlier self-similar models of cluster formation based on a power-law spectrum with $n = -1$ (similar to the CDM power spectrum on cluster mass scales) predict a positive X-ray evolution of rich clusters (Kaiser 1986). Thus, feedback from galaxy formation may not only help explain the observed antibiased gas distribution on the scales of groups and clusters, but also explain the observed X-ray luminosity evolution of these objects.

8. SUMMARY

We have shown how a wealth of information about groups and clusters of galaxies can be obtained by combining optical and X-ray observations. The main results of our work are the following:

1. The distribution of hot gas is anti-biased with respect to the underlying mass on scales of 10^{12}–10^{15} $M_\odot$.

2. The primordial baryon mass fraction is $\sim 30\%$.

3. The mass-to-light ratio of groups and clusters of galaxies is roughly constant at 100–150 $M_\odot/L_\odot$ over a wide range of mass scales.

4. The ratio M_{tot}/M_{lum} monotonically decreases as scales increase from galaxies, to groups, and to rich clusters.

The main cosmological implications of these results are as follows:

1. Hydrodynamics is an important ingredient in the formation of structure on the scales of galaxies to clusters. Gravitational instabilities alone do not reproduce the distribution of dark matter and baryons that are observed.

2. The density of the universe relative to the critical density is $0.13h_{50}^{-1/2} < \Omega < 0.2h_{50}^{-1/2}$, based on standard big bang nucleosynthesis calculations.

3. The observed constant value of M/L_V between groups and rich clusters is consistent with the peaks formalism of biased galaxy formation.

4. The universe actually becomes "brighter" on mass scales between 10^{12}–10^{15} $M_\odot$, not "darker."

A simple scenario consistent with the observations discussed above is one in which the growth of structure is governed by gravitational instability on all scales until the initial epoch of galaxy formation. Feedback from galaxy formation then reheats any residual gas through photoionization and galactic winds. Gas within the shallow potential well of an isolated protogroup will expand (or possibly escape) and attain a flatter distribution than the residual gas within the deeper potential well of a proto-rich cluster.

Over the next decade, the number of groups and clusters with the information presented here should expand dramatically through analysis of *ROSAT*, *ASCA*, *Spectrum X-Gamma*, *XMM*, and *AXAF* observations. A comparison of these observations with hydrodynamic and *N*-body simulations should produce a much clearer picture of the interplay between galaxy formation and the resulting distribution of baryons and dark matter in galaxies, groups, and clusters.

REFERENCES

Arnaud, M., Rothenflug, R., Boulade, O., Vigroux, L., & Vangioni-Flam, E. 1992, A&A, 254, 49
Bardeen, J. M., Bond, J. R., Kaiser, N., & Szalay, A. S. 1986, ApJ, 304, 15
Beers, T. C., Forman, W., Huchra, J. P., Jones, C., & Gebhardt, K. 1991, AJ, 102, 1581
Binney, J., & Tremaine, S. 1987, Galactic Dynamics (Princeton: Princeton Univ. Press)
Bird, C., Dickey, J., & Salpeter, E. E. 1993, ApJ, 404, 81
Blumenthal, G. R., Faber, S. M., Primack, J. R., & Rees, M. J. 1984, Nature, 311, 517
Briel, U. G., Henry, J. P., & Böhringer, H. 1992, A&A, 259, L31
Cavaliere, A., & Fusco-Femiano, R. 1976, Astron. Ap., 49, 137
Cen, R., & Ostriker, J. 1993, ApJ, 417, 404
Cowie, L., Henriksen, M., & Mushotzky, R. 1987, ApJ, 317, 593
Daines, S. 1994, Ph.D. thesis, Univ. Cambridge
David, L. P., Arnaud, K. A., Forman, W., & Jones, C. 1990, ApJ, 356, 32
David, L. P., & Blumenthal, G. 1992, ApJ, 389, 510
David, L. P., Forman, W., & Jones, C. 1991, ApJ, 380, 39
David, L. P., Forman, W., & Jones, C. 1994a, in preparation
David, L. P., Jones, C., Forman, W., & Daines, S. 1994b, ApJ, 428, 544
David, L. P., Slyz, A., Jones, C., Forman, W., Vrtilek, S., & Arnaud, K. 1993, 412, 479

Davis, D., Bird, C., Mushotzky, R., & Odewahn, S. 1994, ApJ, 440, 48
Davis, M., Efstathiou, G., Frenk, C., & White, S. 1985, ApJ, 292, 371
Dressler, A. 1981, ApJ, 243, 26
Edge, A. C., Stewart, G. C., Fabian, A. C., & Arnaud, K. A. 1990, MNRAS, 245, 559
Elbaz, D., Arnaud, M., & Bohringer, H. 1994, A&A, in press
Evrard, A. 1990, ApJ, 363, 349
Evrard, A., Mohr, J., Fabricant, D., & Geller, M. 1994 preprint
Faber, S. M., & Dressler, A. 1977, AJ, 82, 187
Faber, S. M., & Gallagher, J. S. 1978, ARA&A, 17, 135
Fabian, A. C., Nulsen, P. E. J., & Canizares, C. R. 1991, A&A, Rev., 2, 191
Ferguson, H. C., & Sandage, A. 1990, AJ, 100, 1
Forman, W., Jones, C., David, L., Franx, M., Makishima, K., & Ohashi, T. 1993, ApJ, 418, L55
Forman, W., Jones, C., & Tucker, W. 1985, ApJ, 293, 102
Hasinger, G., Boese, Gu., Predehl, P., Turner, T. J., Yusaf, R., George, I., & Rohrbach, G. 1994, MPE/OGIP Calibration Memo CAL/ROS/93-015
Hatsukade, I. 1989, Ph.D. thesis, Osaka Univ.
Heisler, J., Tremaine, S., & Bahcall, J. N. 1985, ApJ, 298, 8
Henriksen, M., & Mamon, G. 1994, ApJ, 421, L63
Henry, J. P., Gioia, I., Maccacaro, T., Morris, S., Stocke, J., & Wolter, A. 1992, ApJ, 386, 408

Henry, J., Briel, U., & Nulsen, P. 1993, preprint
Hill, J. M., Hintzen, P., Oegerle, W. R., Romanishin, W., Lesser, M. P., Eisenhamer, J. D., & Batuski, D. J. 1988, ApJ, 332, L23
Hughes, J. 1989, ApJ, 337, 21
Jones, C., & Forman, W. 1984, ApJ, 276, 38
Jones, C., Stern, C., Forman, W., Breen, J., David, L., Tucker, W., Franx, M., & Fabian, A. C. 1994, ApJ, submitted
Kaiser, N. 1986, MNRAS, 219, 785
———. 1991, ApJ, 383, 104
Kaiser, N., Efstathiou, G., Ellis, R., Frenk, C., Lawrence, A., Rowan-Robinson, M., & Saunders, W. 1991, MNRAS, 252, 1
Melnick, J., & Sargent, W. L. 1977, ApJ, 215, 401
Merritt, D. 1984, ApJ, 276, 26
———. 1987, ApJ, 313, 121
Metzler, C., & Evrard, A. 1994, preprint
Moss, C., & Dickens, R. J. 1977, MNRAS, 178, 701
Mulchaey, J., Davis, D., Mushotzky, R., & Burstein, D. 1993, ApJ, 404, L9
Mushotzky, R. 1994, in Proc. New Horizons of X-ray Astronomy: First Results from ASCA, in press
Ostriker, J. P., & Cowie, L. L. 1981, ApJ, 243, L127

Ostriker, E. C., Huchra, J. P., Geller, M. J., & Kurtz, M. J. 1988, AJ, 96, 1775
Plucinsky, P. P., Snowden, S. L., Briel, U. G., Hasinger, G., & Pfeffermann, E. 1993, ApJ, 418, 519
Ponman, T. J., & Bertram, D. 1993, Nature, 363, 51
Richstone, D., Loeb, A., & Turner, E. 1992, ApJ, 393, 477
Sarazin, C. S. 1986, Rev. Mod. Phys., 58, 1
Shapiro, P., Giroux, M., & Babul, A. 1994, ApJ, 427, 25
Snowden, S. L., McCammon, D., Burrows, D. N., & Mendenhall, J. A. 1994, ApJ, 424, 714
Takahashi, T., et al. 1994, ASCA internal report
The, L. S., & White, S. D. M. 1986, AJ, 92, 1248
Tremaine, S. 1992, Phys. Today, 45, 28
Trinchieri, G., Kim, D. W., Fabbiano, G., & Canizares, C. R. C. 1994, ApJ, 428, 555
Walker, T. P., Steigman, G., Schramm, D. N., Olive, K. A., & Kang, H. 1991, ApJ, 378, 186
White, R. E. 1991, ApJ, 367, 69
White, S. D. M. 1992, in Clusters and Superclusters of Galaxies, ed. A. C. Fabian (Dordrecht: Kluwer), 17
Zabludoff, A., Huchra, J., & Geller, M. 1991, ApJS, 74, 1